Particle simulations of whistler-mode rising-tone emissions triggered by waves with different amplitudes

Mitsuru Hikishima[1,2] and Yoshiharu Omura[2]

Received 1 December 2011; revised 10 February 2012; accepted 12 March 2012; published 28 April 2012.

[1] We perform self-consistent electromagnetic particle simulations to analyze whistler-mode triggered emissions in the magnetosphere. The whistler-mode triggering waves with different wave amplitudes and a constant frequency are injected at the equator. With triggering wave amplitudes greater than the threshold for the nonlinear wave growth, rising-tone emissions are successfully excited near the equator. The detailed time evolutions of amplitudes and frequencies of the rising-tone emissions show similar development. A recent theoretical study found the optimum amplitude of triggering waves for rising-tone emissions. The optimum amplitude condition is confirmed by the simulations. A triggering wave with an amplitude much greater than the optimum amplitude cannot trigger a rising emission. In a process where triggered emissions develop, phase-organized resonant electrons clearly appear in the velocity-phase space, contributing to the nonlinear wave growth. The simulation study shows that amplitudes and frequency sweep rates of triggered emissions do not depend on the amplitude of a triggering wave.

Citation: Hikishima, M., and Y. Omura (2012), Particle simulations of whistler-mode rising-tone emissions triggered by waves with different amplitudes, *J. Geophys. Res.*, *117*, A04226, doi:10.1029/2011JA017428.

1. Introduction

[2] VLF triggered emissions have been detected on the ground, for instance, the Siple and HAARP experiments [*Helliwell and Katsufrakis*, 1974; *Helliwell*, 1983; *Golkowski et al.*, 2010]. Such emissions are triggered by man-made signals which are transmitted on the ground and travel along a magnetic field line. Other forms of magnetospheric triggering waves are Morse code [*Helliwell et al.*, 1964; *Lasch*, 1969], Omega signals from the Omega navigation system [*Gurnett and Inan*, 1988; *Kimura et al.*, 1990], and PLR (power line radiation) from electrical power transmission lines [*Park and Chang*, 1978; *Park and Helliwell*, 1978].

[3] Detailed analyses of whistler-mode chorus propagation by recent observations revealed that the source locations are quite close to the magnetic equatorial plane [*Parrot et al.*, 2003; *Santolik et al.*, 2003]. Man-made signals propagating in the magnetosphere can trigger whistler-mode emissions through cyclotron resonance with energetic electrons. A generation region of the triggered emissions is believed to be close to the magnetic equator [*Inan et al.*, 1977; *Kimura et al.*, 1983; *Bell et al.*, 2000]. Even there are ground observations as a result of field-aligned propagation and in situ satellite observation near the equatorial region, it is difficult to understand the wave phenomena of triggered emission involving nonlinear wave-particle interaction.

[4] Computer experiments have been performed for better understanding of the wave phenomena. The VHS (Vlasov hybrid simulation) code has successfully reproduced the triggered rising and falling tone emissions, with assumption of narrow-band field evolution [*Nunn*, 1990; *Nunn et al.*, 1997, 2003]. It is clarified that resonant currents induced near the equator contribute to formation of the triggered emissions. The importance of resonant current for the generation process of triggered rising-tone emissions has been examined by an electromagnetic electron hybrid code [*Katoh and Omura*, 2006]. A full-particle simulation code, which allows a full evolution of wave-particle interactions, has reproduced triggered rising-tone emissions near the equator [*Hikishima et al.*, 2010]. The simulation showed that seeds of triggered emissions emerge near the triggering wave frequency and that characteristic frequency structures of rising-tone emissions are built up gradually.

[5] A recently developed nonlinear wave growth theory shows that a frequency sweep rate of a rising chorus emission depends on its wave amplitude of an individual wave packet [*Omura et al.*, 2008], and the validity of the theory was confirmed by comparison with a simulation study [*Hikishima et al.*, 2009], and was also demonstrated by observation [*Cully et al.*, 2011]. A statistical study of satellite observations of rising chorus emissions revealed that the frequency sweep rates depend on the plasma density [*Macusova et al.*, 2010] and the tendency is well supported by the backward wave oscillator model [*Trakhtengerts et al.*, 2004]. The numerical simulation study showed the cold

[1]Japan Aerospace Exploration Agency, Ibaraki, Japan.
[2]Research Institute for Sustainable Humanosphere, Kyoto University, Kyoto, Japan.

0148-0227/12/2011JA017428

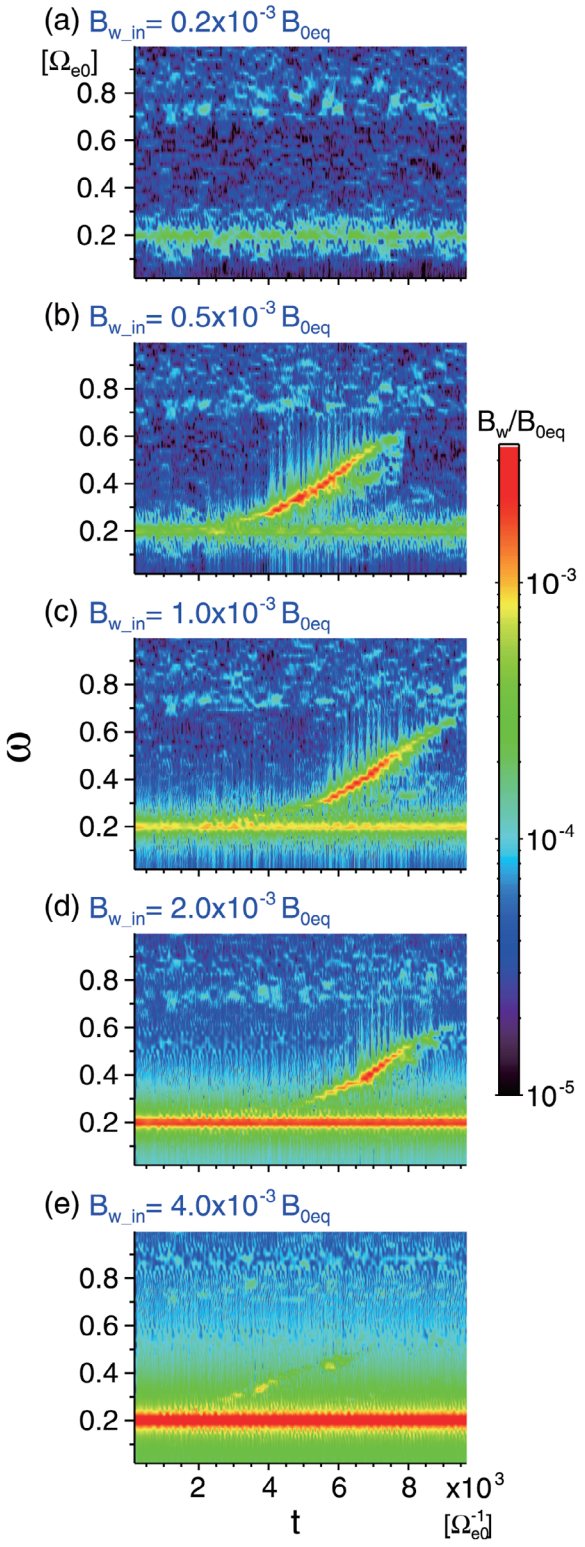

Figure 1. (a–e) Frequency-time spectrograms of transverse wave magnetic field B_w propagating northward near the equator (h = 5 $c\Omega_{e0}^{-1}$), with different triggering wave amplitudes B_{w_in}.

plasma density can be one of the key parameters which affects the frequency sweep rates of triggered rising-tone emissions and showed that variation of input amplitude does not affect them [*Nunn*, 2005]. The electron hybrid simulation focusing on natural chorus generation revealed that density ratio of energetic to cold electrons affects the frequency sweep rate [*Katoh and Omura*, 2011].

[6] Formation of triggered emissions requires a certain threshold to drive the nonlinear wave growth. A threshold experiment for generation of triggered emissions, which was conducted by injections of triggering waves with variable input power [*Helliwell et al.*, 1980], has revealed existence of a threshold level. A triggering wave below a threshold does not produce a triggered emission, and it just undergoes linear amplification [*Nunn*, 2005]. A theoretical study has derived the threshold for the nonlinear wave growth of chorus emissions [*Omura et al.*, 2009], and the estimation of the threshold is found valid for triggered emissions [*Hikishima et al.*, 2010].

[7] Regarding the wave-particle interactions, resonant electrons are stably trapped by the wave potentials. The nonlinear trapping is required for the nonlinear wave growth in an inhomogeneity medium [*Nunn*, 1974; *Omura et al.*, 1991]. The inhomogeneity factor S is determined by terms of spatial gradient of the static magnetic field and frequency variation of the wave. The appropriate condition of inhomogeneity for the nonlinear wave growth of rising tone is found to be $S = -0.4$ [*Omura et al.*, 2008].

[8] In this study, we examine variations of the frequency sweep rates and amplitudes of triggered emissions by injecting triggering waves with different amplitudes from the equator. Through comparison with simulation result, the optimum condition for generation of triggered rising-tone emissions by *Omura and Nunn* [2011] is evaluated.

2. Simulation Model

[9] We use a self-consistent electromagnetic full-particle simulation code to study wave-particle interactions generating whistler-mode triggered emissions in the Earth's inner magnetosphere. The field aligned whistler-mode propagation is assumed in the one-dimensional model. The ambient nonuniform magnetic field in the vicinity of the equatorial region assuming the dipole field is represented by $B_0 = B_{0eq}(1 + ah^2)$ as a parabolic function of a distance h along the field line from the equator, where B_{0eq} is the magnitude of the ambient magnetic field at the equator. To reduce the computation time, we make the simulation system smaller by giving a larger parabolic coefficient $a = 3.7 \times 10^{-6}$ $(c^{-1}\Omega_{e0})^2$ where c is the speed of light, and Ω_{e0} is the equatorial electron gyrofrequency.

[10] Two species of particles, cold electrons and energetic electrons are assumed in the system. The energetic electrons are constructed as a loss-cone distribution based on anisotropic bi-Maxwellian. The parallel and perpendicular thermal velocities $V_{th\|} = 0.23\ c$ and $V_{th\perp} = 0.36\ c$ of energetic electrons give the anisotropy $A(=T_\perp/T_\| - 1) = 1.4$, where $T_\|$ and $T_\perp$ are parallel and perpendicular temperatures, respectively. The cold electron plasma frequency is assumed to be a constant $\omega_{pe} = 5\ \Omega_{e0}$ along the magnetic field line. The density ratio N_h/N_c of energetic electrons to cold electrons are slightly reduced to 6.0×10^{-3}, compared with the

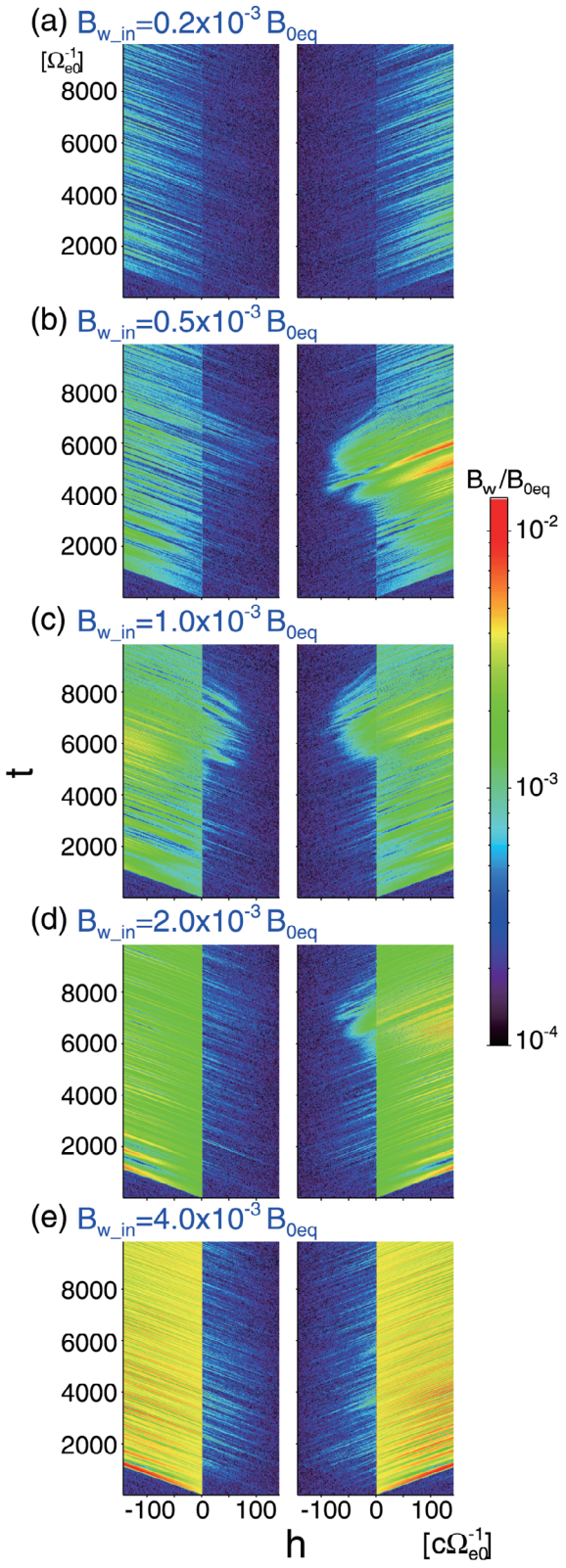

Figure 2. (a–e) Temporal evolutions of northward (right) and southward (left) propagating waves with different triggering wave amplitudes.

previous simulation of triggered emissions [*Hikishima et al.*, 2010]. It is assumed that parallel electric field in the direction of the field line is neglected to prevent a nonphysical diffusion by enhanced electrostatic thermal fluctuations.

[11] Particles having different pitch angles magnetically bounce at each mirror point in the nonuniform dipole magnetic field. Particles with higher pitch angles continue to bounce near the equator in the simulation. We assume a loss cone angle 5.3° at the equator with $L \sim 4$. Though some of particles with lower pitch angles go out of the boundaries at both edges of the system, such particles are re-injected into the simulation system except for particles inside the loss cone. In the presence of a wave-particle interaction in the system, some of particles should be organized in phase. Such particles reflected at boundaries are randomized in gyrophase, which allow to scatter the phase-organized electrons in phase. In this reflection process, the kinetic energy of the particles is conserved, while the coherent structures in the velocity-phase space are destroyed or mitigated for suppression of possible emissions from the reflected electrons. Also, electrons falling into the loss cone at the boundaries are removed from the system at each time step.

3. Simulation Results

3.1. Generation of Triggered Rising-Tone Emissions

[12] Triggered emissions are produced in the equatorial region where wave-particle resonance efficiently occurs. It is assumed that the triggering waves in a whistler-mode are radiated at the magnetic equator in the simulation by injecting a current as the wave source with right-handed polarization. The right-handed whistler-mode waves with constant frequency $\omega = 0.2\ \Omega_{e0}$ are continuously radiated at the equator $h = 0\ c\Omega_{e0}^{-1}$, and the waves then propagate toward higher latitudes along the field line. To study the interaction of wave and counter-streaming resonant particles in detail, we separate the transverse wave magnetic fields B_w into northward and southward propagating right-handed circularly polarized waves.

[13] In the previous simulation study [*Hikishima et al.*, 2010], the triggered emissions were successfully reproduced by propagating triggering waves with amplitude $B_w = 1.3 \times 10^{-3}\ B_{0eq}$. To study effects of the triggering wave amplitude on evolution of triggered emissions, we inject triggering waves with five different amplitudes $B_{w\_in} = 0.2, 0.5, 1.0, 2.0, 4.0(\times 10^{-3})B_{0eq}$. Figure 1 shows frequency-time spectrograms near the equator ($h = 5\ c\Omega_{e0}^{-1}$) for five runs with different amplitudes of the triggering wave. In all cases (Figures 1a–1e), the initial background plasma condition is the same except for the amplitude of the triggering wave. Triggered emissions which form coherent rising tones clearly appear in cases of the triggering wave amplitudes $B_{w\_in} = 0.5 - 2.0(\times 10^{-3})B_{0eq}$ (Figures 1b–1d). Generation of the triggered emissions abruptly disappears in the case of the lowest input amplitude $B_{w\_in} = 0.2 \times 10^{-3}\ B_{0eq}$ in the simulation, the trend is similar to the Siple experiment [*Helliwell et al.*, 1980]. A threshold to drive nonlinear waves growth is expected to be in the range of $B_{w\_in} = 0.2 - 0.5(\times 10^{-3})B_{0eq}$ in the simulation. When the wave amplitude is below the threshold value, there occurs no emission, while the wave amplitude becomes too large ($B_{w\_in} \geq 4.0 \times 10^{-3}\ B_{0eq}$), the emission becomes weak and

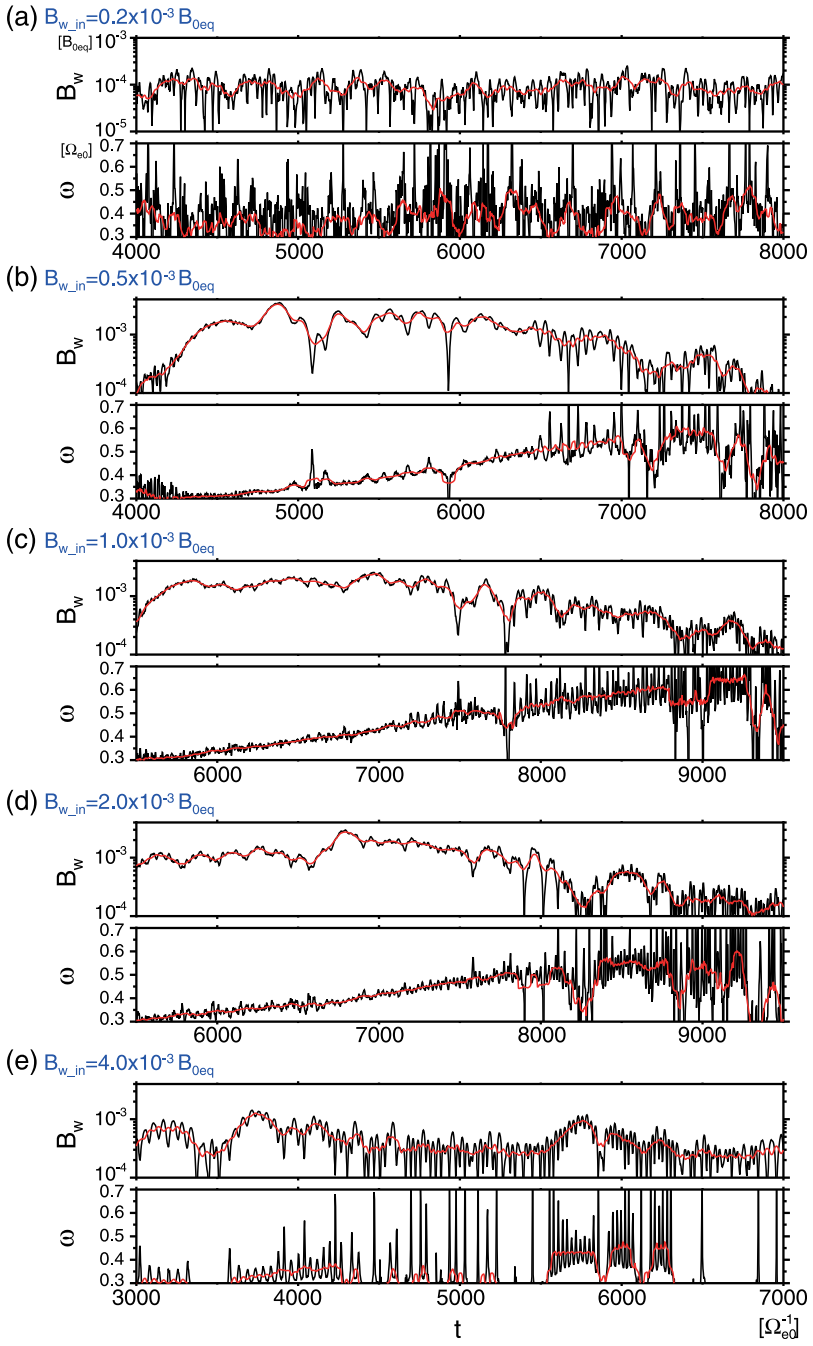

Figure 3. (a–e) Temporal evolutions of amplitudes B_w and frequencies ω of triggered emissions with different triggering wave amplitudes. Smoothed amplitudes and frequencies are plotted by red lines.

unstructured. The simulation results in Figures 1b–1d clearly show that the frequency sweep rates of the emissions are nearly the same regardless of the wave amplitude of the triggering wave. There exists a gap in the frequencies of the triggering wave and the triggered emission in each case. The gap becomes larger as the wave amplitude increases.

[14] Figure 2 shows spatial and temporal variations of the wave amplitudes in the simulation system for cases of five different amplitudes shown in Figure 1. Using the spatial helicity of the wave magnetic fields B_y and B_z which are orthogonal components to the ambient magnetic field, we separate the northward and southward propagating waves and plot them in the right and left panels of Figure 2, respectively. The triggered emissions do not appear at the injection point of triggering wave, but they appear at some distance away from it in the opposite direction of wave propagation. This is because the emissions are generated from the phase-organized electrons that have been interacting with the triggering wave in the upstream region of the electron flux [*Hikishima et al.*, 2010]. After the onset of the triggering waves, there elapses some time before the triggered emission starts. This is the time for resonant electrons to be phase-organized, but the time varies depending on the

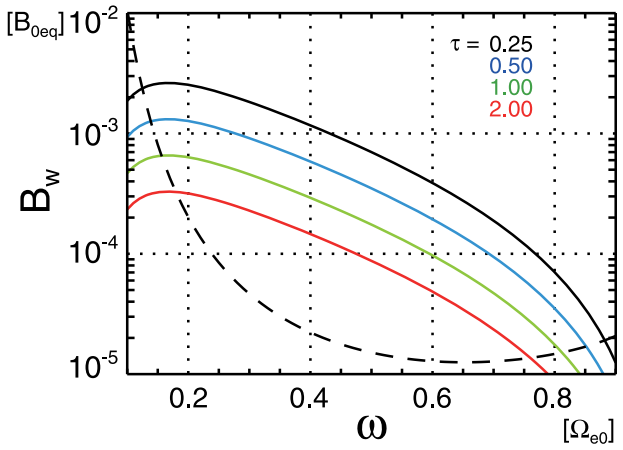

Figure 4. The optimum wave amplitudes (colored solid lines) as a function of wave frequency with different values of τ which are attached at top right, and the threshold amplitude (dashed line) for nonlinear wave growth with $Q = 0.3$.

wave amplitude and the directions of propagation. The emission process depends on the fluctuations of the fields and particle distributions, and thus triggered emissions appear sporadically. Once the emissions are triggered, they exhibit bursty wave growth indicating large growth in time and space.

[15] Figure 3 shows time evolution of the wave amplitude B_w and frequency ω of the triggered emissions propagating northward as observed at a position $h = 5\ c\Omega_{e0}^{-1}$ for the five cases shown in Figure 1. The frequencies of the triggered rising-tone emissions emerge slightly above the frequency of triggering wave, and rise in time.

[16] To identify the characteristics of wave evolution of the triggered emissions by eliminating wavenumbers other than the triggered emissions, we apply the discrete Fourier transformation (DFT) to the wave field over the entire simulation space every time step. We then filter out the wave modes with smaller wavenumbers corresponding to lower frequencies $\omega \leq 0.3\ \Omega_{e0}$ including the triggering waves. We also filter out larger wavenumber components corresponding to higher frequencies than the upper frequency limit of emerging triggered emissions. The spatial wave forms of the triggered emissions are obtained by applying the inverse DFT. We processed the wave data at the reduced sampling frequency $2.45\ \Omega_{e0}$ which can represent frequencies of whistler-mode of interest. The instantaneous wave frequencies at specific times are obtained by calculating the time variation of the wave phase which is obtained from the two orthogonal components of the wave magnetic field. To find the slow variation of the wave amplitude and frequency, we also plotted the smoothed wave amplitudes and frequencies (red lines) obtained by taking a moving average over a time interval $76.8\ \Omega_{e0}^{-1}$ at every time step of $2.56\ \Omega_{e0}^{-1}$.

[17] Figures 3b–3d of the successful triggered emissions show similar characteristics of the wave growth and the frequency variation. The wave amplitudes grow in time gradually and the frequencies increase, and the amplitudes eventually saturate at $B_w \simeq 3.0 \times 10^{-3}\ B_{0eq}$ in the cases (b–d). The waveform of the rising-tone structure is composed of many subpackets with large fluctuation [*Santolik et al.*, 2003], and the frequency almost constantly rises in time. It is noted that frequencies of the triggered emissions increase even after the saturation of the wave amplitudes.

[18] Although the triggering wave amplitudes are different in cases (b–d), the amplitudes of developed triggered emissions show almost the same maximum amplitude $B_w \simeq 3.0 \times 10^{-3}\ B_{0eq}$. Furthermore, the frequency sweep rates are also nearly the same $\partial\omega/\partial t = 9.0 \times 10^{-5}\ \Omega_{e0}^2$ in these cases, which is similar to the simulation result of *Nunn et al.* [2005]. These results are consistent with the nonlinear wave growth theory showing that the frequency sweep rate of a chorus emission depends on its wave amplitude at the moment of generation [*Omura et al.*, 2008, 2009].

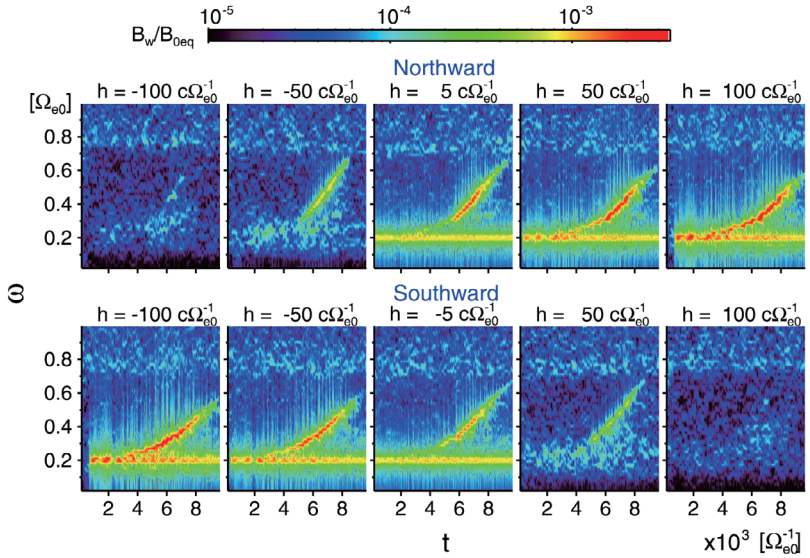

Figure 5. Spatial evolution of frequency-time spectrograms of triggered emissions with triggering wave amplitude $B_{w\_in} = 1.0 \times 10^{-3}\ B_{0eq}$, for (top) northward and (bottom) southward propagating waves.

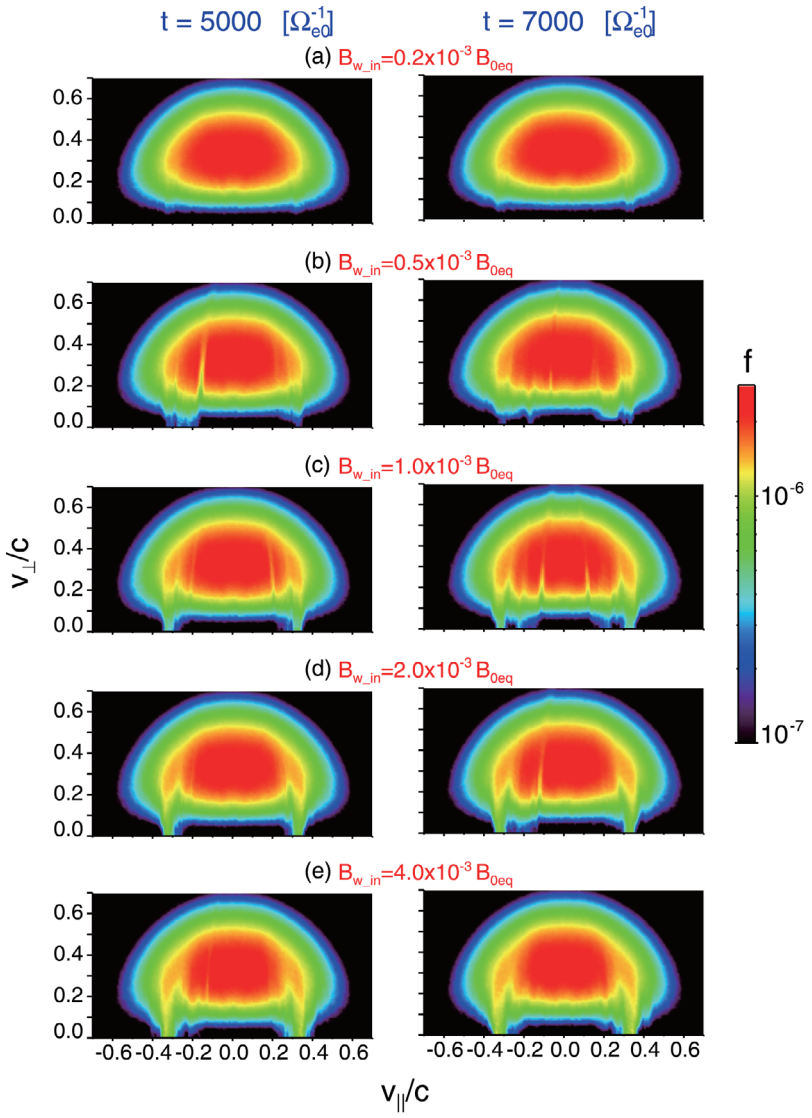

Figure 6. (a–e) Time evolution (t = 5000, 7000 Ω_{e0}^{-1}) of energetic electron velocity distribution function $f(v_{||}, v_\perp)$ with different triggering wave amplitudes at the equatorial region ($h = -10 \sim 10\ c\Omega_{e0}^{-1}$).

3.2. Optimum Wave Amplitude

[19] *Omura and Nunn* [2011] theoretically derived the optimum amplitude that can drive a frequency shift realizing the maximum nonlinear wave growth at the equator. Comparisons with obtained different simulation results of triggered emissions and natural chorus emissions showed good agreements. We now compare the theory with the triggering wave amplitudes that drive triggered emissions in the simulations.

[20] Figure 4 shows the optimum wave amplitudes as a function of wave frequency, which are plotted for different $\tau = 0.25, 0.5, 1.0, 2.0$ (colored lines). The factor τ is the ratio T_N/T_{tr} of the nonlinear transition time T_N for formation of the resonant current and the nonlinear trapping time T_{tr} of resonant electrons. Additionally, the threshold for the nonlinear wave growth is plotted by the dashed line. The optimum wave amplitude and the threshold are functions of the depth factor Q of the electron hole. The factor $Q = 0.3$ is taken for the threshold to be consistent with the simulation results, and it is a reasonable depth of the electron hole in the triggering phase of chorus emissions. In the simulation, triggered rising-tone emissions are successfully excited by triggering waves in the amplitudes $B_{w\_in} = 0.5 - 2.0(\times 10^{-3})B_{0eq}$ with constant frequency $\omega = 0.2\ \Omega_{e0}$. Then, we find that the optimum wave amplitudes with $\tau = 0.25 - 1.0$ agree with the amplitudes of the triggered emissions with rising frequencies as shown in Figures 3b–3d. This implies that triggering of rising tone emissions take place progressively at different frequencies.

[21] The smallest triggering wave amplitude $B_{w\_in} = 0.2 \times 10^{-3}\ B_{0eq}$ cannot excite any triggered emissions, because the triggering wave amplitude is below the threshold and too small to cause the nonlinear wave growth with a rising tone. It is found that a larger triggering wave amplitude (Figure 1e) does not excite triggered emissions with coherent structures. We also carried out several simulation runs with larger triggering wave amplitudes $B_{w\_in} > 2.0 \times 10^{-3}\ B_{0eq}$, which resulted in similar unclear structures (not

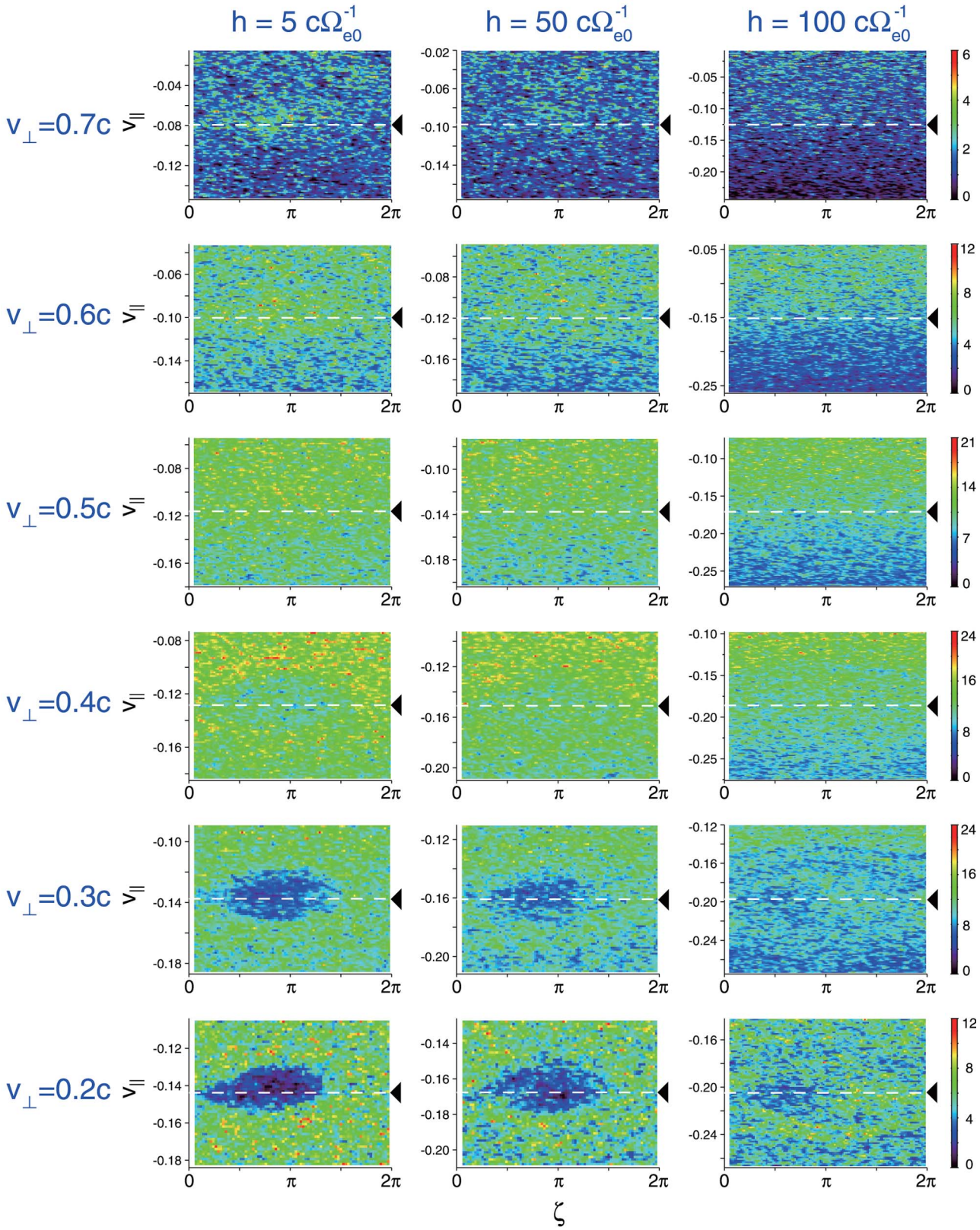

Figure 7. Velocity-phase space density ($v_\parallel$, ζ) of energetic electrons around resonance velocity with perpendicular velocities $v_\perp = 0.2 \sim 0.7\ c$ at positions $h = 5, 50, 100\ c\Omega_{e0}^{-1}$ at $t = 6600\ \Omega_{e0}^{-1}$. The resonance velocity is indicated by dashed line with triangle mark on the right.

shown). The large amplitude of the triggering wave causes a strong modification of the velocity distribution function by nonlinear trapping, which results in formation of a large electron hole. Because of the strong modification of the distribution function, the electron hole does not produce a sufficient resonant current that can induce the frequency change of a rising tone emission. As found in the inhomogeneity ratio S [*Omura et al.*, 2009, equation (10)], the large wave amplitude makes S close to 0, making the electron hole symmetric. The maximum nonlinear wave growth, on the other hand, is due to an asymmetric electron hole with $S = -0.4$, which is attained by the optimum wave amplitude. Therefore, large amplitude waves much larger than the optimum wave amplitude cannot trigger emissions.

3.3. Nonlinear Scattering of Resonant Electrons

[22] Figure 5 shows frequency-time spectrograms of the northward and southward propagating waves at different positions for the case of the triggered emissions with the triggering wave amplitude $B_{w\_in} = 1.0 \times 10^{-3}\ B_{0eq}$ (corresponding Figure 1c). We find that seeds of the rising-tone emissions are generated at $h = -50\ c\Omega_{e0}^{-1}$ for the northward propagation, and $h = 50\ c\Omega_{e0}^{-1}$ for the southward propagation. This implies the process of the frequency increase is through the wave instability at a fixed position, namely, due to an absolute instability. The seeds of the emissions also grow in their amplitudes through propagations, which implies that there also exists a substantial wave growth process. The frequency sweep rates of the emissions change slightly, because the group velocities vary as functions of the frequencies. It is interesting that the triggering waves are also amplified through propagation away from the equator. The nonlinear wave growth mechanism does not work for the constant frequency wave at the equator, while it becomes effective at the off-equatorial regions where the inhomogeneity of the magnetic field contributes to the distortion of the electron hole giving rise to a negative resonant current J_E.

[23] Figure 6 shows the velocity distribution functions of energetic electrons near the equator at different times $t = 5000\ \Omega_{e0}^{-1}$ and $t = 7000\ \Omega_{e0}^{-1}$ for each case with a different triggering wave amplitude as shown in Figure 1. Figure 6a shows the case with a small amplitude of the triggering waves giving no triggered emission. The velocity distribution functions are nearly unchanged compared with the initial distribution function assumed in the simulation, except for slight scatterings at the resonance velocities of the triggering waves propagating northward and southward. In Figures 6b–6d, we can find depletion of electrons at resonance velocities of triggered emissions as well as at those of the triggering waves. Since the resonance velocity decreases with the increase of the wave frequency, the depletion of resonant electrons moves progressively toward the core part of the distribution function at higher pitch angles. At larger perpendicular velocities we find enhancement of the electron flux due to entrapping of the resonant electrons by the wave packet propagating away from the equator. In the large wave amplitude case with no triggered emissions shown in Figure 6e, we only find a large depletion of electrons due to the triggering waves.

[24] Figure 7 shows velocity-phase space density of energetic electrons in ($v_\parallel$, ζ) space in the case of the triggering wave amplitude $B_{w\_in} = 1.0 \times 10^{-3}\ B_{0eq}$ (Figure 5), and the timing is $t = 6600\ \Omega_{e0}^{-1}$ at different locations $h = 5, 50, 100\ c\Omega_{e0}^{-1}$. The ζ is a relative phase angle between the perpendicular velocity of an electron and the wave magnetic field in the transverse plane perpendicular to the static magnetic field. From the top to the bottom panels, we varied the range of the perpendicular velocities $v_\perp = 0.2, 0.3, 0.4, 0.5, 0.6, 0.7\ c$ with a fixed width $\Delta v_\perp = 0.1\ c$ over each of the perpendicular velocities. It should be noted that the contour scale of density is different at each perpendicular velocity.

[25] With rising-tone emissions propagating in space as seen in Figure 5, resonant electrons encounter with the waves having continuously varying wavelength. Therefore, considering a specific spatial range, electrons resonate with slightly different resonance velocities. In order to see clear phase-organized electrons in velocity-phase space, we select electrons existing within a spatial width $\Delta h = 4\ c\Omega_{e0}^{-1}$ (corresponding to a few wavelengths) as centered at the locations h listed above.

[26] We can find clear electron holes around resonance velocity (dashed line) for the smaller perpendicular velocity near the equator (bottom-left panel). The trapped electrons with trapping region are less, nearly void, while untrapped resonant electrons in the phase range $\zeta = \pi \sim 2\pi$ form an intense negative resonant current $J_E (< 0)$ causing the wave growth. The electron hole is asymmetric in phase ζ because of the frequency variation of the triggered emissions giving the inhomogeneity ratio $S \sim -0.4$ as assumed in the nonlinear wave growth theory [*Omura et al.*, 2008].

[27] As the perpendicular velocity becomes large, the trapping region is gradually filled with trapped electrons. Because some of resonant electrons are trapped by the growing wave packet at some distance away from the equator, and they are guided along the resonance velocity with the increasing perpendicular velocity as the particles approach to the equator. Because of the acceleration in the perpendicular direction, the resonant electrons trapped by the wave appear forming an island in the velocity-phase space at large perpendicular velocity as observed in the upper left panels in Figure 7. The trapped electrons receive energy from the wave, while untrapped resonant electrons lose energy to the wave propagating away from the equator. The balance between the electron hole and the electron island in the velocity-phase space determines the saturation of the triggered rising-tone emission.

4. Summary

[28] We have performed self-consistent full-particle simulations for triggered emissions in the equatorial region along the dipole magnetic field. The triggered rising-tone emissions with fine structures are successfully excited by injection of triggering whistler-mode waves with a constant frequency. The characteristics of triggered emissions were examined by various amplitudes of triggering waves. We summarize the simulation results as follows:

[29] 1. There is an amplitude threshold of injected triggering waves for generation of triggered rising-tone emissions.

[30] 2. The optimum amplitude condition [*Omura and Nunn*, 2011] is confirmed by the simulations reproducing triggered emissions.

[31] 3. The triggered rising-tone waves composed of some subpackets are amplified following increasing frequency, and the rising wave frequency is sustained even after amplitude saturation.

[32] 4. The frequency sweep rate of the triggered rising-tone emission is nearly constant regardless of the amplitude of the triggering wave.

[33] 5. A very large triggering wave cannot trigger emissions because of strong modification of the velocity distribution and a suppression of the nonlinear wave growth due to the small inhomogeneity ratio *S*.

[34] 6. Formation of an electron hole is clearly found for resonant electrons at lower perpendicular velocities, resulting in the nonlinear wave growth of triggered rising-tone emissions.

[35] 7. Entrapping of resonant electrons by the growing wave packet of the triggered emission and acceleration of the trapped electrons result in formation of an electron island in the velocity-phase space, causing the saturation of the nonlinear wave growth.

[36] **Acknowledgments.** The computation in this study was performed on the KDK system of RISH at Kyoto University. The present study was supported in part by Grant-in-Aid 23340147 of the Ministry of Education, Science, Sports and Culture of Japan.

[37] Robert Lysak thanks the reviewers for their assistance in evaluating this paper.

References

Bell, T. F., U. S. Inan, R. A. Helliwell, and J. D. Scudder (2000), Simultaneous triggered VLF emissions and energetic electron distributions observed on POLAR with PWI and HYDRA, *Geophys. Res. Lett.*, *27*(2), 165.

Cully, C. M., V. Angelopoulos, U. Auster, J. Bonnell, and O. Le Contel (2011), Observational evidence of the generation mechanism for rising-tone chorus, *Geophys. Res. Lett.*, *38*, L01106, doi:10.1029/2010GL045793.

Golkowski, M., U. S. Inan, M. B. Cohen, and A. R. Gibby (2010), Amplitude and phase of nonlinear magnetospheric wave growth excited by the HAARP HF heater, *J. Geophys. Res.*, *115*, A00F04, doi:10.1029/2009JA014610.

Gurnett, D. A., and U. S. Inan (1988), Plasma wave observations with the dynamics Explorer 1 spacecraft, *Rev. Geophys.*, *37*(4), 407.

Helliwell, R. A. (1983), Controlled stimulation of VLF emissions from Siple Station, Antarctica, *Radio Sci.*, *18*(6), 801.

Helliwell, R. A., and J. Katsufrakis (1974), VLF wave injection into the magnetosphere from Siple Station, Antarctica, *J. Geophys. Res.*, *79*(16), 2511.

Helliwell, R. A., J. Katsufrakis, M. Trimpi, and N. Brice (1964), Artificially stimulated very low frequency radiation from the ionosphere, *J. Geophys. Res.*, *69*(11), 2391.

Helliwell, R. A., D. L. Carpenter, and T. R. Miller (1980), Power threshold for growth of coherent VLF signals in the magnetosphere, *J. Geophys. Res.*, *85*(A7), 3360.

Hikishima, M., S. Yagitani, Y. Omura, and I. Nagano (2009), Full particle simulation of whistler-mode rising chorus emissions in the magnetosphere, *J. Geophys. Res.*, *114*, A01203, doi:10.1029/2008JA013625.

Hikishima, M., Y. Omura, and D. Summers (2010), Self-consistent particle simulation of whistler mode triggered emissions, *J. Geophys. Res.*, *115*, A12246, doi:10.1029/2010JA015860.

Inan, U. S., T. F. Bell, D. L. Carpenter, and R. R. Anderson (1977), Explorer 45 and Imp 6 observations in the magnetosphere of injected waves from the Siple Station VLF transmitter, *J. Geophys. Res.*, *82*(7), 1177.

Katoh, Y., and Y. Omura (2006), A study of generation mechanism of VLF triggered emission by self-consistent particle code, *J. Geophys. Res.*, *111*, A12207, doi:10.1029/2006JA011704.

Katoh, Y., and Y. Omura (2011), Amplitude dependence of frequency sweep rates of whistler mode chorus emissions, *J. Geophys. Res.*, *116*, A07201, doi:10.1029/2011JA016496.

Kimura, I., H. Matsumoto, T. Mukai, K. Hashimoto, T. F. Bell, U. S. Inan, R. A. Helliwell, and J. P. Katsufrakis (1983), EXOS-B/Siple Station VLF wave-particle interaction experiments: 1. General description and wave-particle correlations, *J. Geophys. Res.*, *88*(A1), 282.

Kimura, I., K. Hashimoto, I. Nagano, T. Okada, M. Yamamoto, T. Yoshino, H. Matsumoto, M. Ejiri, and K. Hayashi (1990), VLF observations by the Akebono (EXOS-D) satellite, *J. Geomagn. Geoelectr.*, *42*, 459.

Lasch, S. (1969), Unique features of VLF noise triggered in the magnetosphere by Morse-code dots from NAA, *J. Geophys. Res.*, *74*(7), 1856.

Macusova, E., et al. (2010), Observations of the relationship between frequency sweep rates of chorus wave packets and plasma density, *J. Geophys. Res.*, *115*, A12257, doi:10.1029/2010JA015468.

Nunn, D. (1974), A self-consistent theory of triggered VLF emissions, *Planet. Space Sci.*, *22*, 349.

Nunn, D. (1990), The numerical simulation of VLF nonlinear wave-particle interactions in collision-free plasmas using the Vlasov hybrid simulation technique, *Comput. Phys. Commun.*, *260*, 1.

Nunn, D., Y. Omura, H. Matsumoto, I. Nagano, and S. Yagitani (1997), The numerical simulation of VLF chorus and discrete emissions observed on the Geotail satellite using a Vlasov code, *J. Geophys. Res.*, *102*(A12), 27083.

Nunn, D., A. Demekhov, V. Trakhtengerts, and M. J. Rycroft (2003), VLF emission triggering by a highly anisotropic electron plasma, *Ann. Geophys.*, *21*, 481.

Nunn, D., M. Rycroft, and V. Trakhtengerts (2005), A parametric study of the numerical simulations of triggered VLF emissions, *Ann. Geophys.*, *23*, 3655.

Omura, Y., and D. Nunn (2011), Triggering process of whistler mode chorus emissions in the magnetosphere, *J. Geophys. Res.*, *116*, A05205, doi:10.1029/2010JA016280.

Omura, Y., D. Nunn, H. Matsumoto, and M. J. Rycroft (1991), A review of observational, theoretical and numerical studies of VLF triggered emissions, *J. Atmos. Terr. Phys.*, *53*, 351.

Omura, Y., Y. Katoh, and D. Summers (2008), Theory and simulation of the generation of whistler-mode chorus, *J. Geophys. Res.*, *113*, A04223, doi:10.1029/2007JA012622.

Omura, Y., M. Hikishima, Y. Katoh, D. Summers, and S. Yagitani (2009), Nonlinear mechanisms of lower-band and upper-band VLF chorus emissions in the magnetosphere, *J. Geophys. Res.*, *114*, A07217, doi:10.1029/2009JA014206.

Park, C. G., and D. C. D. Chang (1978), Transmitter simulation of power line radiation effects in the magnetosphere, *Geophys. Res. Lett.*, *5*(10), 861.

Park, C. G., and R. A. Helliwell (1978), Magnetospheric effects of power line radiation, *Science*, *200*(4343), 727, doi:10.1126/science.200.4343.727.

Parrot, M., O. Santolik, N. Cornilleau-Wehrlin, M. Maksimovic, and C. C. Harvey (2003), Source location of chorus emissions observed by Cluster, *Ann. Geophys.*, *21*, 473.

Santolik, O., D. A. Gurnett, J. S. Pickett, M. Parrot, and N. Cornilleau-Wehrlin (2003), Spatio-temporal structure of storm-time chorus, *J. Geophys. Res.*, *108*(A7), 1278, doi:10.1029/2002JA009791.

Trakhtengerts, V. Y., A. G. Demekhov, E. E. Titova, B. V. Kozelov, O. Santolik, D. Gurnett, and M. Parrot (2004), Interpretation of Cluster data on chorus emissions using the backward wave oscillator model, *Phys. Plasmas*, *11*(4), 1345.

M. Hikishima, Japan Aerospace Exploration Agency, 2-1-1 Sengen, Tsukuba, Ibaraki 305-8505, Japan. (hikishima.mitsuru@jaxa.jp)

Y. Omura, Research Institute for Sustainable Humanosphere, Kyoto University, Uji, Kyoto 611-0011, Japan. (omura@rish.kyoto-u.ac.jp)